AIAA 2006-3119
Approximate Solution for Pressure Drop in Microchannels of Arbitrary Cross-Sections

M. Bahrami,
Department of Mechanical Engineering
University of Victoria
Victoria, BC, Canada, V8W3P6

M. M. Yovanovich, J. R. Culham
Department of Mechanical Engineering
University of Waterloo
Waterloo, ON, Canada N2L 3G1

9th AIAA/ASME Joint Thermophysics and Heat Transfer Conference
June 5 – 8, 2006, San Francisco, CA

Approximate Solution for Pressure Drop in Microchannels of Arbitrary Cross-Section

Majid Bahrami*
Department of Mechanical Engineering, University of Victoria,
Victoria, BC, V8W 3P6, Canada.

M. Michael Yovanovich† and J. Richard Culham‡
Department of Mechanical Engineering, University of Waterloo,
Waterloo, ON, N2L 3G1, Canada.

This paper outlines an approximate solution for determining the pressure drop of fully-developed, laminar, single-phase flow in microchannels of arbitrary cross-section. Using a "bottom-up" approach, it is shown that for constant fluid properties and flow rate in fixed cross-section channels, the Poiseuille number is only a function of geometrical characteristics of the cross-section, i.e., perimeter, area, and polar moment of inertia. The model is validated with experimental data for rectangular, trapezoidal, and triangular microchannels. The model is also compared against numerical results for a wide variety of channel cross-sections including: hyperellipse, trapezoid, sine, square duct with two adjacent round corners, rhombic, circular sector, circular segment, annular sector, rectangular with semi-circular ends, and moon-shaped channels. The model predicts the pressure drop for the cross-sections listed within 8 percent of the values published.

Nomenclature

A	=	cross-sectional area, m^2	***Greek***		
a, b, c	=	channel cross section dimensions, m	α	=	aspect ratio trapezoidal duct, b/a
D_h	=	hydraulic diameter $4A/P$, m	β	=	dimensionless parameter
$E(\cdot)$	=	complete elliptic integral of 2nd kind	ε	=	aspect ratio, $0 < c/b \leq 1$
f	=	Fanning friction factor, $2\overline{\tau}/\rho\overline{w}^2$	ρ	=	fluid density, kg/m^3
I_p	=	polar moment of inertia, m^4	μ	=	fluid viscosity, $kg/m.s$
I_p^*	=	specific polar moment of inertia, I_p/A^2	τ	=	wall shear stress, N/m^2
n	=	exponent, hyperellipse parameter	ϕ	=	trapezoidal channel angle, rad
P	=	perimeter, m	Δp	=	pressure drop, Pa
Po	=	Poiseuille number	$\Gamma(\cdot)$	=	gamma function
$Re_{\sqrt{A}}$	=	Reynolds number, $\rho\overline{w}\sqrt{A}/\mu$	***Subscripts***		
w	=	fluid velocity, m/s	$\sqrt{A}$	=	sqrt of cross-sectional area, m
$\overline{w}$	=	mean fluid velocity, m/s	L	=	Lateral

*Assistant Professor, Mem. AIAA,ASME.
†Professor Emeritus, Fellow AIAA,ASME.
‡Associate Professor, Mem. ASME.

I. Introduction

Micro electromechanical systems (MEMS) fabrication technologies make it possible to build micro fluidic, silicon-based microchannels of different cross-sections in microsystems such as micro heat sinks, micro biochips, micro reactors and micro nozzles. Microchannels are also being used as gas delivery systems and heat exchangers in fuel cell technologies. Microchannels offer high surface area per volume ratios, high heat transfer coefficients, and low thermal resistances.[1] Microchannels can be produced directly by techniques such as chemical etching on silicon wafers. As a result, the cross-section of the channels depends on a variety of factors, such as the crystallographic nature of the silicon used. When a KOH-anisotropic etching technique is employed, microchannels with fixed cross-sections are obtained.[2] The shape of the cross-section depends on the orientation of the silicon crystal planes. For instance, the microchannels etched in 100 or in 110 silicon will have a trapezoidal cross-section with an apex angle of 54.7° imposed by the crystallographic morphology of the silicon or a rectangular cross-section, respectively.[2]

In recent years, a large number of experimental studies have focused on pressure drop of laminar flow of liquids in microchannels with various cross-sections. However, published results are often inconsistent. According to Pfund et al.,[3] some of these authors conducted experiments in non-circular microchannels, but compared their pressure drop data with the classical values of fRe=16 or 64 of circular pipes. Recently, Liu and Garimella[4] and Wu and Cheng[5] conducted experiments in *smooth* rectangular and trapezoidal microchannels, respectively. They reported that the Navier-Stokes equations are valid for laminar flow in smooth microchannels (micron size dimensions). Some of the discrepancies observed in the published data can be explained within the limits of continuum fluid mechanics and are due to wall roughness of microchannels. Bahrami et al.[6] developed an analytical model that predicts the observed trends in randomly *rough* microchannels.

Finding analytical solutions for many practical singly-connected cross-sections, such as trapezoidal microchannels, is complex and/or impossible. In many engineering applications such as basic design and optimization, it is often required to obtain the trends and a reasonable estimate of the pressure drop. Muzychka and Yovanovich[7,8] introduced a geometrical mapping for predicting the pressure drop of fully-developed, laminar flow in non-circular channels; in which non-circular ducts are mapped into equivalent rectangular channels. They proposed the use of the square root of cross-sectional area as the characteristics length instead of the hydraulic diameter. Comparing the rectangular mapping model with published numerical results, they have demonstrated that the $f\,\mathrm{Re}_{\sqrt{A}}$, is a weak function of the geometry of the cross-section. Their model,[7] however, requires an equivalent rectangle which may not be applicable to the general case of "arbitrary cross-section".

The goal of this paper is to develop an accurate approximate model that can predict the pressure drop for channels of arbitrary cross-section. The proposed model is compared with experimental and/or numerical data for channels such as: *rectangular, elliptical, triangular, hyperellipse, trapezoid, sine, square duct with two adjacent round corners, rhombic, circular sector, circular segment, annular sector, rectangular with semi-circular ends*, and *moon-shaped*. After successful validation of the model with these channels, the analysis can be expanded to the general case of *arbitrary cross-section*. The model estimates the pressure drop of the cross-sections listed above within approximately 8% accuracy and provides a powerful tool for basic designs, parametric studies, and optimization analyses required for applications such as in microchannel heat exchangers and heat sinks.

II. Proposed Model

The assumptions of the present model can be summarized as:

- fully developed, steady-state, laminar, and continuum flow
- constant cross-sectional area A and constant perimeter P

- constant fluid properties, i.e., liquid or low-speed gas
- negligible rarefaction, slip-on-the-wall and surface effects, body forces such as gravity, centrifugal, Coriolis, and electromagnetic.

For such a flow, the Navier-Stokes equations reduce to the momentum equation. This is Poisson's equation in one or two dimensions depending on the cross-sectional geometry. In this case, the "source" term in Poisson's equation is the constant pressure drop along the length of the duct, Δp. The governing equation for fully-developed laminar flow in a constant cross-sectional area channel is:[9]

$$\nabla^2 w = \frac{1}{\mu}\frac{dp}{dz} \qquad \text{with} \qquad w = 0 \text{ on boundary} \tag{1}$$

where w and z are the fluid velocity and the flow direction, respectively. The boundary condition for the velocity is the no-slip condition on the wall. The velocity profile is constant in the longitudinal direction; thus the pressure gradient applied at the ends of the channel must be balanced by the shear stress on the wall of the channel

$$\overline{\tau} P L = \Delta p \; A \tag{2}$$

where

$$\overline{\tau} = \frac{1}{A_L}\int_{\Gamma} \tau \; dA_L$$

where A_L is the lateral surface area of the duct and $\overline{\tau}$ is the mean wall shear stress.

The proposed model is based on the analytical solution of the elliptical channel, not because it is likely to occur in practice, but rather to utilize the unique geometrical property of its velocity solution.

In this section, first we show through analysis that the square root of the cross-sectional area is a "more appropriate" choice for the characteristic length scale of arbitrary cross-section channels.

Using the analytical solution,[10,11] the *mean velocity* for the laminar fluid flow in elliptical ducts is:

$$\overline{w} = \frac{b^2 c^2}{4\left(b^2 + c^2\right)}\frac{\Delta p}{\mu \; L} \tag{3}$$

where b and c are the major and minor semi-axes of the cross-section, $b \geq c$. An aspect ratio is defined for the elliptical microchannel

$$0 < \epsilon \equiv \frac{c}{b} \leq 1 \tag{4}$$

For an elliptical microchannel, the cross-sectional area and the perimeter are: $A = \pi bc$ and $P = 4b \; E\left(\sqrt{1-\epsilon^2}\right)$, where $E\left(x\right) = \int_0^{\pi/2} \sqrt{1 - x^2 \sin^2 t} \; dt$ is the complete elliptic integral of the second kind. The mean velocity can be presented in terms of the aspect ratio, ϵ,

$$\overline{w} = \frac{c^2}{4\left(1+\epsilon^2\right)}\frac{\Delta p}{\mu L} \tag{5}$$

Combining Eqs. (2) and (5), the mean wall shear stress becomes:

$$\overline{\tau} = \frac{4\left(1+\epsilon^2\right)\overline{w}}{c^2}\frac{\mu A}{P} \tag{6}$$

Substituting for the area and perimeter of the elliptical duct, the mean wall shear stress becomes:

$$\overline{\tau} = \frac{\pi\left(1+\epsilon^2\right)}{E\left(\sqrt{1-\epsilon^2}\right)}\frac{\mu \overline{w}}{c} \tag{7}$$

A relationship can be found between the minor axis c and the aspect ratio from the cross-sectional area, $c = \sqrt{A\varepsilon/\pi}$. Substituting c into Eq. (7), one finds

$$\overline{\tau} = \frac{\pi\sqrt{\pi}\left(1+\epsilon^2\right)}{\sqrt{\epsilon}E\left(\sqrt{1-\epsilon^2}\right)}\frac{\mu\overline{w}}{\sqrt{A}} \tag{8}$$

It is conventional to use the ratio of area over perimeter $D_h = 4A/P$, known as the *hydraulic diameter*, as the characteristic length scale for non-circular channels. However, as can be seen in Eq. (8), a more appropriate length scale is the *square root of area,* $\sqrt{A}$.

With the square root of area $\sqrt{A}$ as the characteristic length scale, a non-dimensional wall shear stress can be defined as:

$$\overline{\tau}^* \equiv \frac{\overline{\tau}\sqrt{A}}{\mu\overline{w}} = \frac{\pi\sqrt{\pi}\left(1+\epsilon^2\right)}{\sqrt{\epsilon}E\left(\sqrt{1-\epsilon^2}\right)} \tag{9}$$

It should be noted that the right hand side of Eq. (9) is only a function of the aspect ratio (geometry) of the channel.

Using Eq. (8), the Fanning friction factor, defined as $f \equiv 2\overline{\tau}/\rho\overline{w}^2$, for elliptical microchannels becomes

$$f = \frac{2\pi\sqrt{\pi}\left(1+\epsilon^2\right)}{\sqrt{\epsilon}E\left(\sqrt{1-\epsilon^2}\right)}\frac{\mu}{\rho\overline{w}\sqrt{A}} \tag{10}$$

The Reynolds number can be defined based on the square root of area, $\sqrt{A}$, as

$$Re_{\sqrt{A}} = \frac{\rho\overline{w}\sqrt{A}}{\mu} \tag{11}$$

Equation (10) becomes

$$f\,\mathrm{Re}_{\sqrt{A}} = \frac{2\pi\sqrt{\pi}\left(1+\epsilon^2\right)}{\sqrt{\epsilon}\;E\left(\sqrt{1-\epsilon^2}\right)} \tag{12}$$

Similar to $\overline{\tau}^*$, $fRe_{\sqrt{A}}$ is only a function of the geometry of the channel. Thus, a relationship can be found between the non-dimensional friction factor $\overline{\tau}^*$ and $fRe_{\sqrt{A}}$

$$fRe_{\sqrt{A}} = 2\overline{\tau}^* \tag{13}$$

The method described for the elliptical channels, can be applied for other shapes such as rectangular channels. Therefore, it is left to the reader to follow the steps for other cross-sections. Following the same steps, the friction factor Reynolds number product based on the square root of the cross-sectional area for rectangular ducts is:[11]

$$fRe_{\sqrt{A}} = \frac{12}{\left[1 - \frac{192}{\pi^5}\epsilon\tanh\left(\frac{\pi}{2\epsilon}\right)\right](1+\epsilon)\sqrt{\epsilon}} \tag{14}$$

The original analytical solution for the mean velocity in rectangular channels is in the form of a series. However, when $\epsilon = 1$ (square), the first term of the series gives the value $fRe_{\sqrt{A}} = 14.132$ compared with the exact value (full series solution) of 14.23. The maximum difference of approximately 0.7% occurs at $\epsilon = 1$. For smaller values of ϵ, the agreement with the full series solution is even better.[11] Therefore, only the first term is employed in this study.

Figure 1 shows the comparison of the analytical solutions of $fRe_{\sqrt{A}}$, for elliptical and rectangular cross-sections based on hydraulic diameter and the square root of area. As can be seen, the selection of the square root of area as the characteristic length leads to similar trends in $fRe_{\sqrt{A}}$ for elliptical and rectangular channels with identical cross-sectional area.

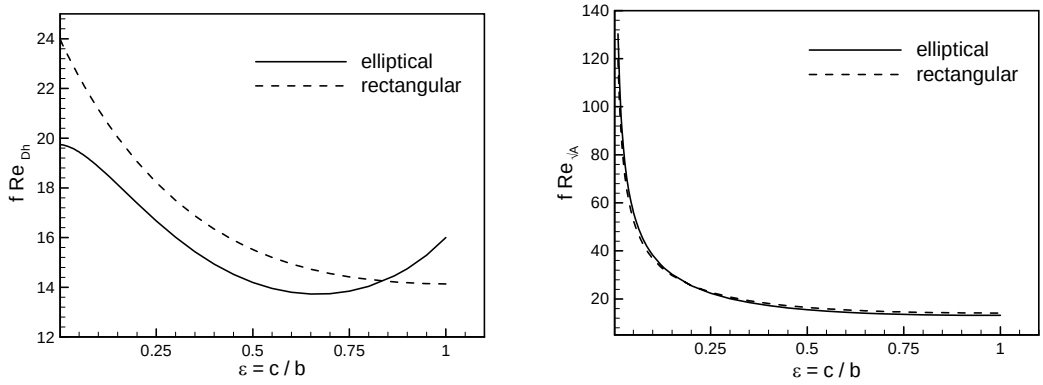

Figure 1. Comparison between analytical solutions of fRe for elliptical and rectangular ducts using a) hydraulic diameter and b) square root of area as characteristic length.

Elliptical and rectangular cross-sections cover a wide range of singly-connected microchannels. With the similarity in the trends of the solutions for these cross-sections, one can conclude that a general, *purely geometrical*, relationship may exist that predicts $fRe_{\sqrt{A}}$ for arbitrary singly-connected cross-sections. Based on this observation, an *approximate model* is developed in this paper.

Torsion in beams and fully-developed, laminar flow in ducts are similar in the sense that the governing equation for both problems is Poisson's equation, Eq. (1). Comparing various singly connected cross-sections, Saint-Venant 1880 found that the torsional rigidity can be approximated by replacing the given shaft by the shaft of an elliptic cross-section having the same cross-sectional area and the same polar moment of inertia as the given shaft.[12] Using Saint-Venant's concept, the present model employs the analytical solution of the elliptical duct to approximate the pressure drop in ducts of arbitrary cross-section.

The polar moment of inertia, $I_p = \int_A \left(x^2 + y^2\right) dA$, for an ellipse is

$$I_p = \frac{\pi bc\left(b^2 + c^2\right)}{4} \tag{15}$$

Equation (5) can be re-arranged in terms of the polar moment of inertia, about its center, as follows:

$$\frac{\Delta p}{L} = \frac{16\pi^2 \mu \overline{w}}{A^3} I_p = \frac{16\pi^2 \mu \overline{w}}{A} I_p^* \tag{16}$$

where $I_p^* = I_p/A^2$ is a non-dimensional geometrical parameter which we call the *specific polar moment of inertia.* Combining Eqs. (2) and (16), one can write

$$\overline{\tau} = \frac{16\pi^2 \mu \overline{w}}{\sqrt{A}} \frac{\sqrt{A}}{P} I_p^* \tag{17}$$

Note that $\sqrt{A}/P$ is also a non-dimensional parameter. Using Eq. (17), the Fanning friction factor can be determined

$$f\,\mathrm{Re}_{\sqrt{A}} = 32\pi^2\ I_p^* \frac{\sqrt{A}}{P} \tag{18}$$

The right hand side of Eq. (18) only contains general geometrical characteristics of the cross-section, i.e., I_p, A, and P. These geometrical parameters can easily be calculated for any conduit (arbitrary cross-section). Therefore, the proposed model postulates that for constant fluid properties and flow rate in a channel of

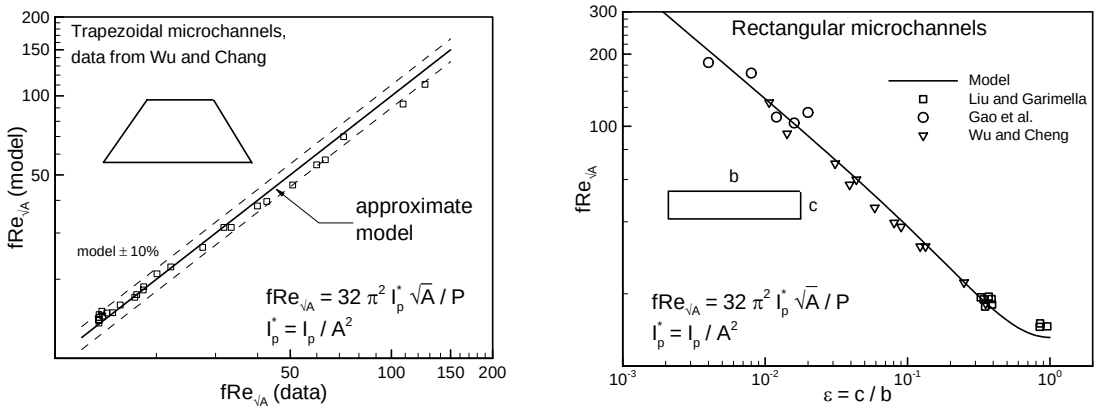

Figure 2. Comparison of present model and experimental data for trapezoidal [5] and rectangular [4,5,14] microchannels.

fixed cross-section, $f\,\mathrm{Re}_{\sqrt{A}}$ is only a function of the non-dimensional geometrical parameter, $I_p^*\sqrt{A}/P$, of the cross-section. To apply the present model, the following steps must be taken:

- find the center of geometry of the cross-section
- calculate geometrical parameters of the channel, i.e., perimeter P, cross-sectional area A, and polar moment of inertia I_p about the center of geometry, and determine $f\,\mathrm{Re}_{\sqrt{A}}$ using Eq. (18).

Normally to find the friction factor: first Poisson's equation must be solved (numerically for most cross-sections) to find the velocity field, then the mean velocity and the mean wall shear stress, and finally $fRe_{\sqrt{A}}$ must be determined. Applying the present model, on the other hand, one only needs to compute the non dimensional parameter $I_p^*\sqrt{A}/P$ of the channel to determine $fRe_{\sqrt{A}}$. It clearly shows the convenience of the proposed model.

For more complex cross-sections such as moon-shaped ducts, the geometry often consists of simpler parts where the moment of inertia is known or easily calculated. The moment of inertia of the complex geometries about an axis can be found by *algebraic sum* of the moments of inertia of "simpler" geometries.[13]

III. Comparison With Experimental Data

In this section, the present model is compared against experimental data collected by several researchers[4, 5, 14] for microchannels. The reported accuracy of the experimental data is on the order of 10%.

Wu and Cheng[5] conducted experiments and measured the friction factor of laminar flow of deionized water in a number of smooth silicon microchannels of trapezoidal cross-section over a range of Reynolds numbers.

The frictional resistance $fRe_{\sqrt{A}}$ is not a function of Reynolds number, i.e., it remains constant for the laminar regime as the Reynolds number varies. Therefore, the experimental data for each set are averaged over the laminar region. As a result, for each experimental data set, one value of $fRe_{\sqrt{A}}$ can be obtained. The microchannels considered by Wu and Cheng[5] cover a wide range of geometrical parameters, i.e., $0.71 \leq \epsilon \leq 97.70$ and $0 \leq \beta \leq 1$ [see Eq. (23)], as a result the data include trapezoidal, triangular, and rectangular microchannels. Figure 2a shows the comparison between all data of Wu and Cheng[5] and the proposed model. The $\pm 10\%$ bounds of the model are also shown in the plot, to better demonstrate the agreement between the data and the model.

Liu and Garimella[4] carried out experiments and measured the friction factor in rectangular microchannels. They did not observe any scale-related phenomena in their experiments and concluded that the conventional theory can be used to predict the flow behavior in microchannels in the range of dimensions considered. They[4] measured and reported the relative surface roughness of the channels to be negligible, thus their channels can be considered smooth. Gao et al.[14] experimentally investigated laminar fully developed flow in rectangular microchannels. They designed their experiments to be able to change the height of the channels tested while the width remained constant at 25 mm. They conducted experiments with several channel heights. Gao et al.[14] measured the roughness of the channel and reported negligible relative roughness, thus their channels can be considered smooth.

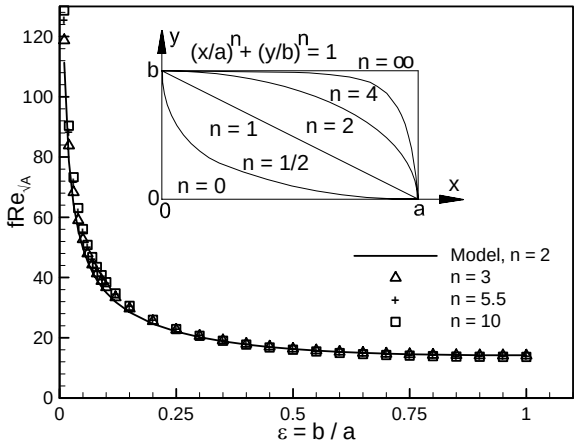

Figure 3. Geometry and fRe predicted by model for hyperellipse channels for n = 3, 5.5, 10.

Following the same method described for trapezoidal data, the reported values of $fRe_{\sqrt{A}}$ for rectangular microchannels[4,14] are averaged (over laminar region) and plotted against the model in Fig. 2b. As shown in Fig. 2b, the collected data cover a wide range of the aspect ratio $\varepsilon = c/b$, almost three decades; also the relative difference between the data and the model is within the uncertainty of the experiments.

IV. Comparison with Numerical Results

In this section, the present model is compared with numerical results[9,15] for available cross-sections. Geometrical parameters needed to apply the model for some of the cross-sections are reported for most geometries. The following relationship is used to convert the Reynolds number Fanning friction factor product based on D_h to $\sqrt{A}$

$$fRe_{\sqrt{A}} = \frac{P}{4\sqrt{A}}\, fRe_{D_h} \tag{19}$$

where $D_h = 4A/P$ is the hydraulic diameter of the channel.

A. Hyperellipse Channel

A hyperellipse, in the first quadrant, is described by $y = b\left[1 - (x/a)^n\right]^{1/n}$, where a and b are characteristic dimensions along the x and y axes, respectively, see Fig. 3. The effect of the parameter n on the shape of the hyperellipse channel is also shown in Fig. 3. When $n = 1$, the hyperellipse yields a rhombic duct $(a > b)$, and a square for $(a = b)$; at $n = 2$, the channel is elliptical $(a > b)$, and circular $(a = b)$; $n > 3$, it is

a rectangular ($a > b$) or a square ($a = b$) channel with rounded corners; and when $n \to \infty$, it approaches a full rectangle/square duct.[16] The cross-sectional area of a hyperellipse can be calculated from:

$$A = 4a^2\varepsilon \frac{\sqrt{\pi}\Gamma\left(\frac{n+1}{n}\right)}{4^{1/n}\Gamma\left(\frac{n+2}{2n}\right)} \tag{20}$$

where $\Gamma(\cdot)$ is the gamma function and $\varepsilon = b/a$. The perimeter of the hyperellipse does not have a closed form solution and must be calculated numerically from, $P = 4\int_0^a \sqrt{1 + (dy/dx)^2}dx$. The polar moment of inertia of a hyperellipse about its center of geometry (origin) is:

$$I_p = 4a^4 \left[\frac{3\varepsilon^3\Gamma\left(\frac{n+1}{n}\right)\Gamma\left(\frac{3}{n}\right) + \varepsilon\Gamma\left(\frac{n+3}{n}\right)\Gamma\left(\frac{1}{n}\right)}{3n\Gamma\left(\frac{n+4}{n}\right)} \right] \tag{21}$$

It should be noted that the model is based on the analytical solution for elliptical channel which is a

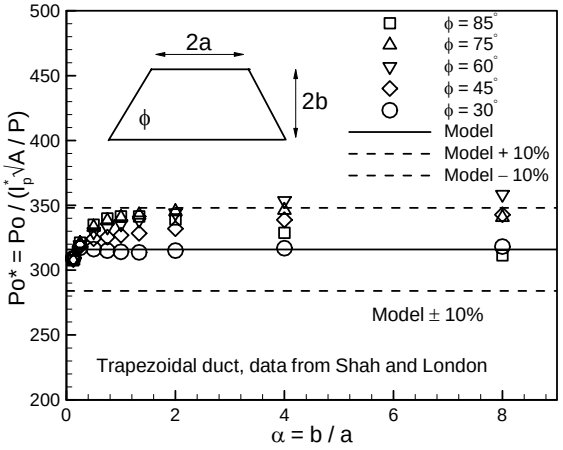

Figure 4. Comparison between non-dimensional $fRe_{\sqrt{A}}$ predicted by the model and numerical results of Shah and London [9] for trapezoidal channel.

hyperellipse with $n = 2$. Also, the maximum difference between the elliptical ($n = 2$) and rectangular ($n \to \infty$) ducts analytical solutions is less than 8%. As a result, it can be concluded that the difference between the $f\,\mathrm{Re}_{\sqrt{A}}$ predicted by the present model and that of a hyperellipse with any other value of $2 \le n \le \infty$ is less than 8%, as shown in Fig. 3. Figure 3 also represents the $f\,\mathrm{Re}_{\sqrt{A}}$ values predicted by the model for several values of $n = 3, 5.5, 10$ over aspect ratios $0.01 \le \varepsilon = b/a \le 1$.

B. Trapezoidal Channel

Trapezoidal cross-section is an important geometry since some microchannels are manufactured with trapezoidal cross-sections as a result of the etching process in silicon wafers. Furthermore, in the limit when the top side length goes to zero, it yields an isosceles triangle. At the other limit when top and bottom sides are equal, it becomes rectangle/square. The cross-sectional area, perimeter, and polar moment of inertia (about

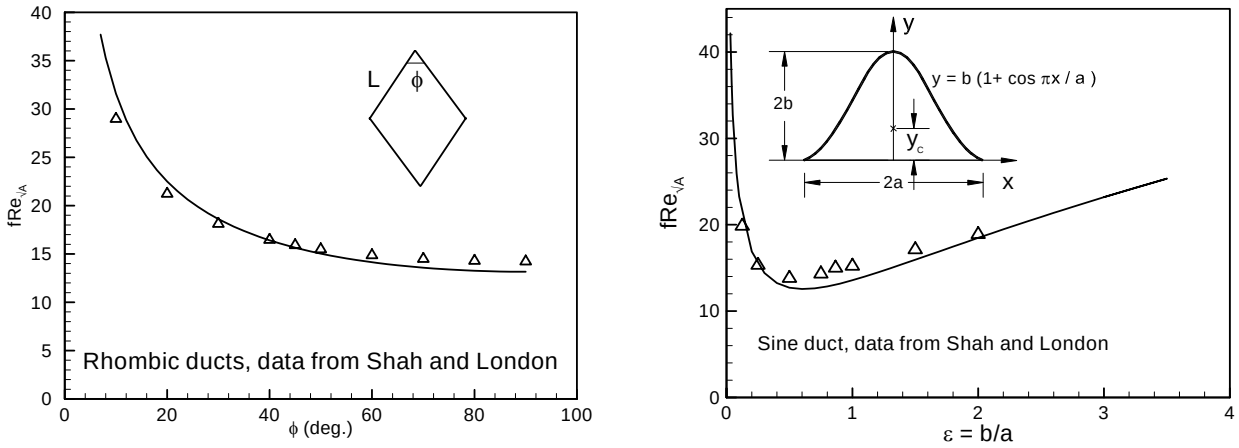

Figure 5. Comparison of present model and numerical values [9] for rhombic and sine channels.

its center) are; $A = 4b^2\epsilon$, $P = 4b\left(\epsilon + \sqrt{\epsilon^2 - \beta\epsilon^2 + 1}\right)$, and

$$\begin{aligned} I_p &= \frac{A^2\left[2\left(3\epsilon^2+1\right)+\beta\left(1-3\epsilon^2\right)\right]}{36\ \epsilon} \\ \epsilon &\equiv \frac{1}{\alpha}+\frac{1}{\tan\phi} \quad \text{and} \quad \beta \equiv 1-\frac{1}{\epsilon^2\tan^2\phi} \end{aligned} \tag{22}$$

where $\alpha = b/a$. Using Eq. (18), one can find $fRe_{\sqrt{A}}$:

$$fRe_{\sqrt{A}} = \frac{8\pi^2\left(3\epsilon^2+1\right)+\beta\left(1-3\epsilon^2\right)}{9\sqrt{\epsilon}\left(\epsilon+\sqrt{\epsilon^2-\beta\epsilon^2+1}\right)} \tag{23}$$

Shah and London[9] reported numerical values for fRe_{D_h} for laminar fully developed flow in a trapezoidal channel. They presented fRe_{D_h} values as a function of $\alpha = b/a$ for different values of angles ϕ.

Figure 4 shows the comparison between Eq. (23) and the numerical data reported by Shah and London.[9] For convenience, the comparison is presented using a non-dimensional form of $fRe_{\sqrt{A}}$

$$Po^* = \frac{f\,\mathrm{Re}_{\sqrt{A}}}{I_p^*\sqrt{A}/P} \tag{24}$$

Note that based on the model, $Po^* = 32\pi^2 = 315.83$, see Fig. 4. Table 1 also shows the comparison between the approximate model and the numerical data reported by Shah and London.[9] As can be seen, except for a few points, the agreement between the approximate model and the numerical values is reasonable (less than 10%).

C. Rhombic Channel

Cross-sectional area, perimeter, and specific polar moment of inertia of a rhombic duct can be determined from; $A = L^2\sin\phi$, $P = 4L$, and $I_p^* = 1/6\sin\phi$, where L is the side of the rhombic duct. Using Eq.(18), $fRe_{\sqrt{A}}$ for the rhombic duct becomes

$$f\,\mathrm{Re}_{\sqrt{A}} = \frac{4\pi^2}{3\sqrt{\sin\phi}} \tag{25}$$

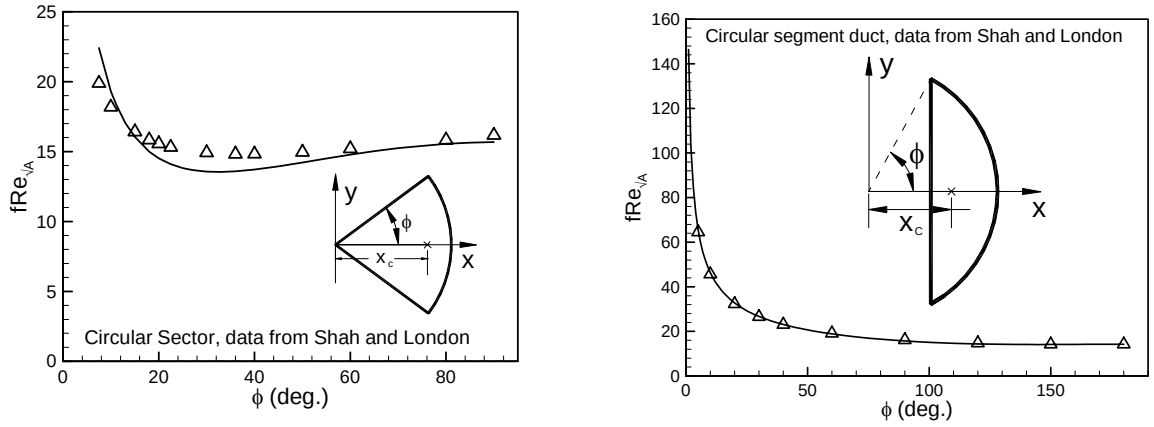

Figure 6. Comparison of model and numerical values [9] for circular sector and circular segment channels.

Figure 5a shows the comparison between numerical results[9] and Eq. (25). The maximum difference between the present model and numerical results is on the order of 8%.

D. Sine Channel

The sine channel is represented by $y = b\,(1 + \cos \pi x/a)$. The center of geometry, area, and perimeter of a sine duct can be found from; $y_c = 3b/4$, $A = 2ab$, and $P = 2a + 4aE(\pi\sqrt{-\varepsilon^2})$, respectively. The $fRe_{\sqrt{A}}$ becomes:

$$f\,\mathrm{Re}_{\sqrt{A}} = 4\sqrt{2}\pi^2 \left[\frac{\pi^2 - 6}{6\pi^2\varepsilon} + \frac{13\varepsilon}{96}\right] \frac{\sqrt{\varepsilon}}{1 + 2E\left(\pi\sqrt{-\varepsilon^2}\right)/\pi} \tag{26}$$

where $E\,(\cdot)$ is the complete elliptic integral of the second kind and $\varepsilon = b/a$. Figure 5b shows the comparison between numerical results from[9] and Eq. (26). The model presents the trends of the numerical results with n difference of 9.3%.

E. Circular Sector Channel

The center of geometry, area, polar moment of inertia, and perimeter of a circular sector duct can be found from; $x_c = 2a \sin\phi/3\phi$, $A = a^2\phi$, $I_p = a^4\left(9\phi^2 - 8\sin^2\phi\right)/18\phi$, and $P = 2a\,(1 + \phi)$, respectively. The $fRe_{\sqrt{A}}$ becomes:

$$f\,\mathrm{Re}_{\sqrt{A}} = \frac{8\pi^2\sqrt{\phi}\left(9\phi^2 - 8\sin^2\phi\right)}{9\phi^3\,(1 + \phi)} \tag{27}$$

Figure 6a shows the comparison between numerical results from Shah and London[9] and Eq. (27). The model presents the trends of the numerical results with a mean difference of 7.6%.

F. Circular Segment Channel

The cross-sectional area and perimeter of a circular segment duct can be found from; $A = a^2\,(\phi - 0.5\sin 2\phi)$ and $P = 2a\,(\phi + \sin\phi)$. The polar moment of inertia about the center of geometry is:

$$I_p = a^4\left[\frac{\phi}{2} - \frac{\sin 2\phi\left(1 + 2\cos^2\phi\right)}{12} - \frac{\left(2\sin\phi - \cos\phi\sin 2\phi\right)^2}{9\,(\phi - 0.5\sin 2\phi)}\right]$$

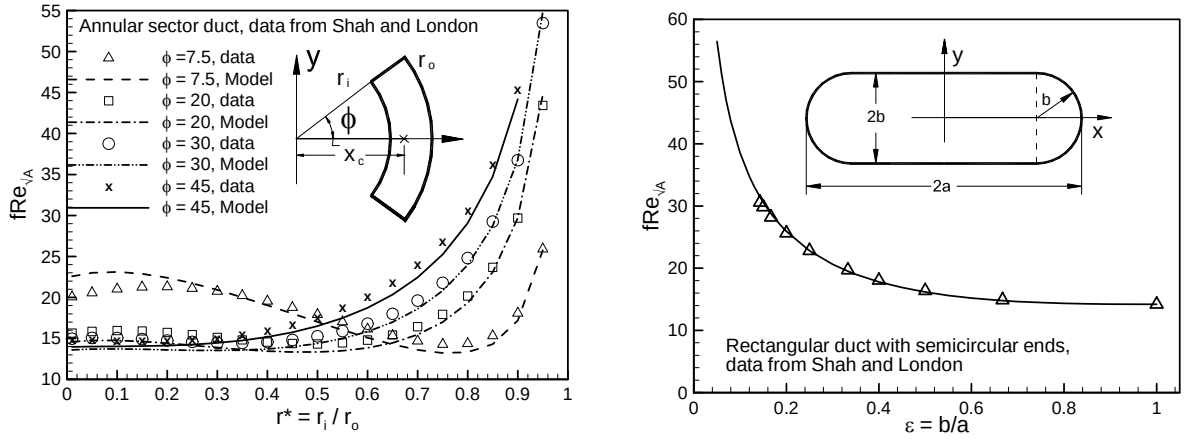

Figure 7. Comparison of model and numerical values [9] for annular sector and rectangular duct with semi-circular ends.

Figure 6b represents the comparison between the numerical results in Shah and London[9] and the present model. As seen, the present model shows excellent agreement with the numerical result with a maximum relative difference of 3.1%.

G. Annular Sector Channel

The center of geometry, area, polar moment of inertia, and perimeter of a circular sector duct can be found from; $A = \phi r_0^2 \left(1 - r^{*2}\right)$ and $P = 2r_0 \left[\left(1 + r^*\right)\phi + 1 - r^*\right]$

$$\begin{aligned} x_c &= \frac{2r_0 \sin\phi}{3\phi} \frac{1 - r^{*3}}{1 - r^{*2}} \\ I_p^* &= \frac{\frac{1}{2}\left(1 - r^{*4}\right) - \frac{4}{9}\left(\frac{\sin\phi}{\phi}\right)^2 \frac{\left(1 - r^{*3}\right)^2}{1 - r^{*2}}}{\phi\left(1 - r^{*2}\right)^2} \end{aligned}$$

where $r^* = r_i/r_o$. The $fRe_{\sqrt{A}}$ becomes:

$$f\,\mathrm{Re}_{\sqrt{A}} = \frac{16\pi^2\sqrt{\phi\left(1 - r^{*2}\right)}\left[\frac{1}{2}\left(1 - r^{*4}\right) - \frac{4}{9}\left(\frac{\sin\phi}{\phi}\right)^2 \frac{\left(1 - r^{*3}\right)^2}{1 - r^{*2}}\right]}{\phi\left(1 - r^{*2}\right)^2\left[\left(1 + r^*\right)\phi + 1 - r^*\right]} \tag{28}$$

Figure 7a represents the comparison between the numerical results in Shah and London[9] and the present model, Eq. (28). The present model shows good agreement with the numerical results for $2 \le \phi \le 75$ degree, with a maximum relative difference of less than 8%.

H. Rectangular Channel with Semi Circular Ends

The cross-sectional area, perimeter, and polar moment of inertia of a circular sector duct can be found from; $A = a^2\left[4\varepsilon\left(1 - \varepsilon\right) + \pi\varepsilon^2/2\right]$ and $P = 2a\left(2 - 2\varepsilon + \pi\varepsilon\right)$ and

$$I_p = a^4\left[\frac{4\varepsilon\left(1 - \varepsilon\right)\left[\varepsilon^2 + \left(1 - \varepsilon\right)^2\right]}{3} + \varepsilon^4\left(\frac{\pi}{4} - \frac{8}{9\pi}\right) + \frac{\pi\varepsilon^2}{2}\left(1 - \varepsilon + \frac{4\varepsilon}{3\pi}\right)^2\right] \tag{29}$$

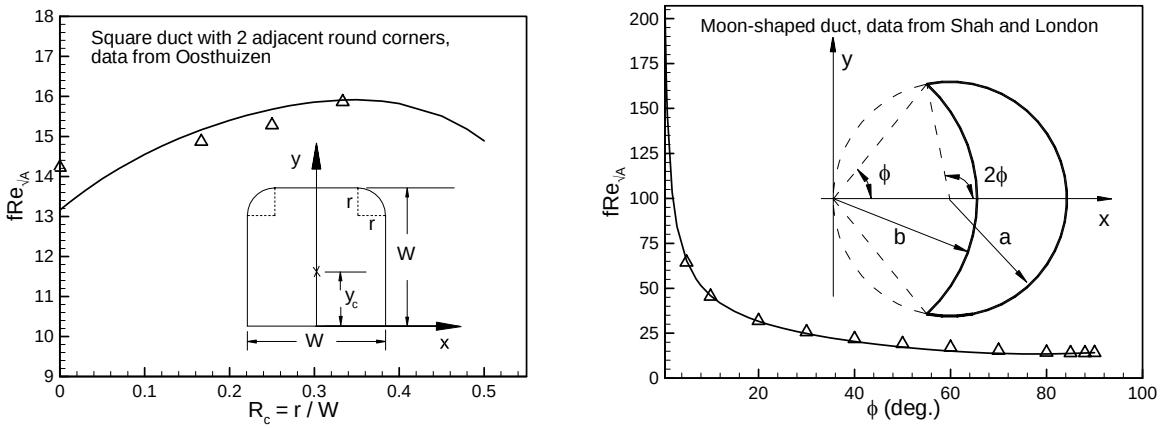

Figure 8. Comparison of present model and numerical values for square duct with 2 adjacent round corners [15] and moon-shaped [9] channels.

Figure 7b represents the comparison between the numerical results of Shah and London[9] and the present model. As seen, the present model shows excellent agreement with the numerical result with a maximum relative difference of 2.7%.

I. Other Cross-Sections

The present model is also compared with numerical results for square minichannels with two adjacent rounded corners[15] and moon-shaped ducts[9] in Fig. 8, with relative differences of 2.5% and 4.8%, respectively.

V. Conclusion

The pressure drop of fully-developed, laminar, single-phase flow in smooth channels of arbitrary cross-sections is investigated. It is shown that the square root of area $\sqrt{A}$, as the characteristic length scale, is superior to the conventional hydraulic diameter, D_h. An approximate model is introduced, based on the analytical solution for an elliptical duct, and compared against experimental and numerical data for several cross-sections. This "bottom-up" approach clearly shows a common trend in all geometries considered.

The present model is only a function of geometrical parameters of the cross-section, i.e., area, perimeter, and polar moment of inertia. The proposed model is compared with experimental and numerical results for channels with cross-sections including: rectangle, triangle, hyperellipse, trapezoid, sine, square duct with two adjacent round corners, rhombic, circular sector, circular segment, annular sector, rectangular with semi-circular ends, and moon-shaped. The model successfully predicts the pressure drop for a wide variety of shapes with a difference on the order of 8%.

Acknowledgments

The authors gratefully acknowledge the financial support of the Centre for Microelectronics Assembly and Packaging, CMAP and the Natural Sciences and Engineering Research Council of Canada, NSERC.

References

[1]Yang, C., Wu, J., Chien, H., and Lu, S., "Friction Characteristics of Water, R-134a, and Air in Small Tubes," *Microscale Thermophysical Engineering*, Vol. 7, 2003, pp. 335–348.

[2]Morini, G. L., "Laminar-to-Turbulent Flow Transition in Microchannels," *Microscale Thermophysical Engineering*, Vol. 8, 2004, pp. 15–30.

[3]Pfund, D., Rector, D., Shekarriz, A., Popescu, A., and Welty, J., "Pressure Drop Measurements in a Microchannel," *AICHE Journal*, Vol. 46, No. 8, 2000, pp. 1496–1507.

[4]Liu, D. and Garimella, S., "Investigation of Liquid Flow in Microchannels," *Journal of Thermophysics and Heat Transfer, AIAA*, Vol. 18, No. 1, 2004, pp. 65–72.

[5]Wu, H. Y. and Cheng, P., "Friction Factors in Smooth Trapezoidal Silicon Microchannels With Different Aspect Ratios," *Int. J. Heat Mass Transfer*, Vol. 46, 2003, pp. 2519–2525.

[6]Bahrami, M., Yovanovich, M. M., and Culham, J. R., "Pressure Drop of Fully Developed, Laminar Flow in Rough Microtubes," *ASME J. of Fluid Engineering (in press). Also ASME 3rd Int. Conf. on Microchannels, July 13-15, U. of Toronto, Canada, Paper No. ICMM2005-75108*, 2005.

[7]Muzychka, Y. S. and Yovanovich, M. M., "Solution of Poisson Equation Within Sigly and Doubly Connected Prismatic Domains," *Paper No. AIAA97-3880, Proceedings of National Heat Transfer Conference, Baltimore, MD, Aug. 10-12*, 1997.

[8]Muzychka, Y. S. and Yovanovich, M. M., "Laminar Flow Friction and Heat Transfer in Non-Circular Ducts and Channels Part 1: Hydrodynamic Problem," *Proceedings of Compact Heat Exchangers, A Festschrift on the 60th Birthday of Ramesh K. Shah, Grenoble, France*, 2002, pp. 123–130.

[9]Shah, R. K. and London, A. L., *Laminar Flow Forced Convection In Ducts*, chap. 10, Academic Press, New York, 1978.

[10]White, F. M., *Viscous Fluid Flow*, chap. 3, McGraw-Hill, Inc., New York, 1974.

[11]Yovanovich, M. M., *Advanced Heat Conduction*, chap. 12, In Prepararti on.

[12]Timoshenko, S. P. and Goodier, J. N., *Theory of Elasticity*, chap. 10, McGraw-Hill, Inc., New York, 1970.

[13]Hibbeler, R. C., *Engineering Mechanics Statics and Dynamics*, Pearson, Prentice Hall, Upper Saddle River, NJ 07458, U.S.A, 2004.

[14]Gao, P., Person, S. L., and Favre-Marinet, M., "Scale Effects on Hydrodynamics and Heat Transfer in Two-Dimensional Mini and Microchannels," *Int. J Thermal Sciences*, Vol. 41, 2002, pp. 1017–1027.

[15]Oosthuizen, P. H., "Flow and Heat Transfer in a Square Minichannel with Rounded Corners," *ASME 3rd International Conference on Microchannels, July 13-15, U. of Toronto, Canada*, 2005.

[16]Yovanovich, M. M., Burde, S. S., and Thompson, C. C., "Thermal Constriction Resistance of Arbitrary Planar Contacts With Constant Flux," *AIAA, Paper No. 76-440*, Vol. 56, 1976, pp. 126–139.

Table 1. MODEL VS DATA [9], TRAPEZOIDAL CHANNELS

				$fRe_{\sqrt{A}}$[a]		
α^*	fRe_{D_h}	ϵ	β	model	[9]	%dif.
			ϕ=85°			
8	17.474	0.212	0.830	23.384	23.054	1.41
4	16.740	0.337	0.933	18.563	19.325	-4.11
2	15.015	0.587	0.978	14.516	15.587	-7.38
4/3	14.312	0.837	0.989	13.318	14.398	-8.11
1	14.235	1.087	0.994	13.203	14.274	-8.11
3/4	14.576	1.421	0.996	13.774	14.825	-7.63
1/2	15.676	2.087	0.998	15.806	16.770	-6.10
1/4	18.297	4.087	1.000	22.648	23.038	-1.72
1/8	20.599	8.087	1.000	33.804	32.926	2.60
			ϕ=75°			
8	14.907	0.393	0.535	15.745	16.982	-7.85
4	14.959	0.518	0.732	14.725	16.142	-9.62
2	14.340	0.768	0.878	13.499	14.754	-9.30
4/3	14.118	1.018	0.931	13.244	14.365	-8.46
1	14.252	1.268	0.955	13.520	14.576	-7.81
3/4	14.697	1.601	0.972	14.304	15.311	-7.04
1/2	15.804	2.268	0.986	16.430	17.332	-5.49
1/4	18.313	4.268	0.996	23.165	23.505	-1.47
1/8	20.556	8.268	0.999	34.155	33.254	2.64
			ϕ=60°			
8	13.867	0.702	0.324	13.540	15.364	-13.47
4	13.916	0.827	0.513	13.544	15.162	-11.95
2	13.804	1.077	0.713	13.623	14.842	-8.95
4/3	13.888	1.327	0.811	13.953	14.960	-7.21
1	14.151	1.577	0.866	14.484	15.392	-6.26
3/4	14.637	1.911	0.909	15.384	16.230	-5.49
1/2	15.693	2.577	0.950	17.482	18.241	-4.34
1/4	18.053	4.577	0.984	23.908	24.184	-1.15
1/8	20.304	8.577	0.995	34.582	33.735	2.45
			ϕ=45°			
8	13.301	1.125	0.210	14.669	15.921	-8.53
4	13.323	1.250	0.360	14.796	15.874	-7.28
2	13.364	1.500	0.556	15.123	15.899	-5.13
4/3	13.541	1.750	0.673	15.573	16.194	-3.99
1	13.827	2.000	0.750	16.125	16.691	-3.51
3/4	14.260	2.333	0.816	16.973	17.492	-3.06
1/2	15.206	3.000	0.889	18.869	19.377	-2.69
1/4	17.397	5.000	0.960	24.760	24.952	-0.77
1/8	19.743	9.000	0.988	34.958	34.268	1.97
			ϕ=30°			
8	12.760	1.857	0.130	17.923	18.058	-0.75
4	12.782	1.982	0.236	18.013	18.077	-0.35
2	12.875	2.232	0.398	18.277	18.235	0.23
4/3	13.012	2.482	0.513	18.633	18.509	0.66
1	13.246	2.732	0.598	19.062	18.961	0.53
3/4	13.599	3.065	0.681	19.720	19.672	0.25
1/2	14.323	3.732	0.785	21.220	21.249	-0.14
1/4	16.284	5.732	0.909	26.178	26.295	-0.44
1/8	18.479	9.732	0.968	35.489	34.747	2.09